

Experimental study on the interactions between wave groups in double-wave-group focusing

Cite as: Phys. Fluids **35**, 037118 (2023); doi: [10.1063/5.0142042](https://doi.org/10.1063/5.0142042)

Submitted: 10 January 2023 · Accepted: 22 February 2023 ·

Published Online: 14 March 2023



View Online



Export Citation



CrossMark

Binzhen Zhou (周斌珍),¹ Kanglixi Ding (丁康礼玺),¹ Jiahao Wang (王家豪),¹ Lei Wang (王磊),^{1,a)}
Peng Jin (金鹏),² and Tianning Tang (唐天宁)³

AFFILIATIONS

¹School of Civil Engineering and Transportation, South China University of Technology, Guangzhou 510641, China

²School of Marine Science and Engineering, South China University of Technology, Guangzhou 510641, China

³Department of Engineering Science, University of Oxford, Oxford OX1 3PJ, United Kingdom

^{a)} Author to whom correspondence should be addressed: wangleim@scut.edu.cn

ABSTRACT

Nonlinear interactions in wave-group focusing are regarded as one of the main mechanisms in the generation of destructive extreme waves. In real seas, the wideband bimodal state is a typical configuration, containing interactions within a single wave group and between different wave groups. The former has been well uncovered under the assumption of narrow bandwidth, but the latter is poorly understood. In this paper, physical experiments are conducted to reveal the physics of double-wave-group focusing considering various energy distributions. Superposed wavemaker signals generated by the iteration method are applied to produce a double-wave-group focusing with the interactions being decomposed. Results of the wavelet-based bicoherence spectrum show that double-wave-group focusing is distinguished from the linear superposition of two single-wave-group focusing mainly in the nonlinear interactions induced by the second-order sum harmonics. Under the assumption of equivalent energy, interactions of the second-order sum harmonics between the lower frequency group and higher frequency group cannot be ignored in swell-dominated states, and lesser linear interactions and stronger nonlinear interactions are observed while the spectral distribution of the double-wave-group is more asymmetrical. This work is anticipated to contribute to the understanding of the generation mechanism of extreme waves driven by strong nonlinearity.

Published under an exclusive license by AIP Publishing. <https://doi.org/10.1063/5.0142042>

I. INTRODUCTION

In recent years, as giant waves,¹ known as one of the most astonishing marine disasters,^{2,3} take place with a frequency much higher than expected,^{4–7} studies on extreme waves become a hot issue. Several physical mechanisms to reveal these extreme events have been summarized as geometrical or spatial focusing, spatial–temporal focusing, wave–current interaction, modulation instability, soliton collision, and so on. Among these, spatial–temporal focusing due to the dispersive nature of water waves is a classic mechanism yielding wave-energy concentration.⁸ This effect, which can occur at the sea surface, can also be reproduced easily in a laboratory experiment and be the main research method for generating extreme waves.

Significant progress in the explanation of the focused wave mechanism has been made. Under the assumption of linear mechanism, focusing waves were regarded as a sum of independent monochromatic waves by adjusting the initial phase of each wave component.^{9,10} However, in a real sea state, the wave components focusing is a nonlinear phenomenon.¹¹ Based on this fact, Benjamin and Feir¹² proposed

a nonlinear mechanism named modulation instability, also known as the third-order nonlinear action, in which high-frequency harmonics were considered to be bound to the carrier wave, propagating at a speed close to the carrier wave. Modulation instability was widely accepted to be the most important mechanism for extreme wave generation without considering topography, current, or wind.^{13–15} Further, Gibson and Swan¹⁶ found that the third-order resonant effects dominated changes to both the amplitude and the dispersive properties of the wave group. Later, wavelet-based bicoherence was introduced to ocean engineering to study the nonlinear phase coupling in the nonlinear wave–wave interactions by Dong *et al.*¹⁷ Tao *et al.*¹⁸ numerically proved that, besides the generally accepted modulation instability, wave group interaction is another nonlinear mechanism leading to different kinds of extreme waves in different time scales. Li *et al.*¹⁹ developed a second-order theory to explain the interaction of deterministic surface gravity wave packets considering an abrupt depth transition and pointed out that these processes were generally dominated by the superharmonic terms in intermediate water depths.

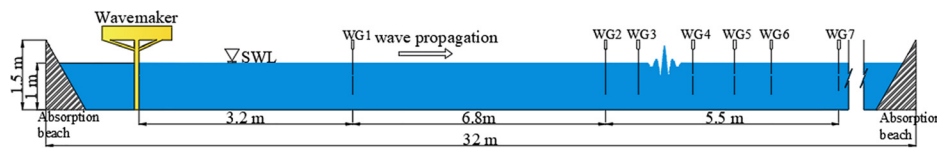


FIG. 1. Sketch of the wave flume and experimental setup.

Through the analysis of the horizontal asymmetries and wave group contractions found in two distinct datasets, Tang *et al.*²⁰ discussed nonlinear physics changes in the average shape of the largest events. Recently, Xie *et al.*²¹ numerically studied the resonant interactions between two gravity wave trains and found that the bending and splitting of the crests and troughs were caused by the energy transfer from the primary waves to obliquely propagating high-frequency resonant waves with lower phase velocity due to exact resonance interaction.

Various approaches are put forward to generate focused waves in a physical experiment. Chaplin²² summarized three kinds of dispersion-focusing methods: the phase velocity method, the group velocity method, and the reverse dispersion method. Then, Fitzgerald *et al.*²³ used this method to investigate the steady state of transient waves. While once the wave steepness becomes finite, the effect of nonlinearity on the wave evolution is not to be ignored, making the focused position shift from the prescribed.^{24,25} To address this issue, iterative methods were proposed, in which the initial phases²⁶ or both the initial phases and the amplitudes^{27,28} corresponding to different wave frequency components were iteratively corrected, finally fulfilling the correction of the wavemaker signals. Later, Buldakov *et al.*²⁹ developed a methodology that only iteratively corrected the linearized part of the wave spectrum, quite beneficial to focus on the assumed focused position more quickly. This method is widely preferred in physical experiments.

A great effort has been made in the unimodal sea state, a configuration with a relatively narrow bandwidth. However, in the real sea state, there are many circumstances accompanied by bimodal spectra.^{30,31} The severe storm or typhoon can lead the initial unimodal swell-dominated sea state to form a bimodal state with swell and wind-sea mixed. In such a bimodal state, two wave groups with different peak frequencies coexistences, in which besides the interactions within a single wave group, there are also interactions between different wave groups. Whether these two interaction mechanisms are identical is not clearly stated. Therefore, the objective of the present work is to investigate the interactions between wave groups based on double-wave-group focusing experiments. The novelties are three-folded. First, different from the traditional method, the wavemaker signals of the corresponding single-wave-group focusing obtained by the iterative method are linearly

superposed, which overcomes the predicament that the interactions between two wave groups and within the single wave group cannot be decomposed. Second, the difference caused by the interactions between different wave groups and within a single wave group is compared in the time domain and frequency domain. Nonlinear interactions coupled in the double-wave-group focusing are further analyzed. Third, the influence of spectral distribution on the energy transfer and the participation in nonlinear interaction at the focused position is also explored.

The rest of the paper is arranged as follows. Section II introduces the experimental setup and the wave conditions. The generation method of focused waves and analytical methodology are described in Sec. III. Nonlinear interactions inducing focusing in double-wave-group focusing are analyzed in Sec. IV, and the influences of spectral distribution on energy transfer and the nonlinear interactions at the prescribed focused position are compared in Sec. V.

II. EXPERIMENTAL CONDITIONS

A. Experimental setup

The wave-group focusing experiments, considering double-wave-group focusing and its corresponding single-wave-group focusing, were carried out in the wave flume at the Ship and Ocean Engineering Laboratory, at South China University of Technology, China. The wave flume is 32 m long, 1 m wide, and 1.5 m deep. The waves were generated by a piston-type wavemaker on one side. The far end and left hand side of the wavemaker were equipped with wave-absorbing systems to eliminate the influence of wave reflection. The schematic diagram of the wave flume is given in Fig. 1. The working water depth d is kept at 1.0 m. Seven resistance-type wave gauges (WGs) were arranged to record surface elevation at 50 Hz with absolute accuracy of order ± 1 mm. WG1 was 3.2 m away from the wavemaker (defined as $x_{\text{amp}} = 3.2$ m) to measure the input wave parameters. WG2 was at the assumed focused location, defined as $x_b = 10$ m. WG3–WG7 were movable from 10 to 16 m away from the wavemaker (Fig. 2) depending on the actual focused facts of double-wave-group focusing. Before measurement, each wave gauge was strictly examined for soundness and then calibrated to ensure reliable performance. During the

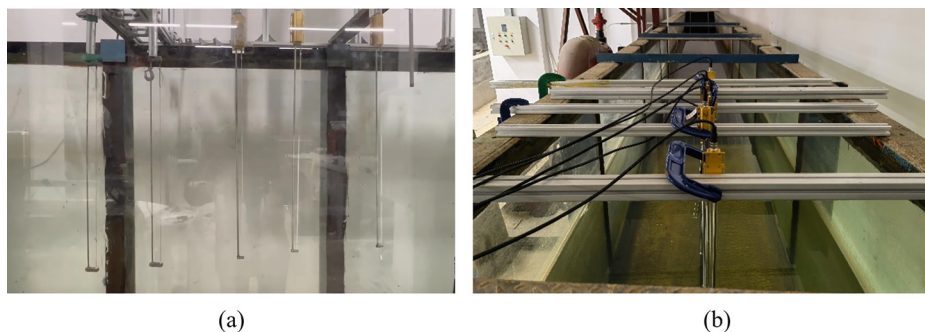


FIG. 2. Arrangement of wave gauges. (a) Side view and (b) top view.

TABLE I. Main parameters in single-wave-group focusing tests.

(a) Lower frequency (LF) group				
Case	f_{p1} (Hz)	$f_{L1} \sim f_{H1}$ (Hz)	A_{b1} (m)	$k_{p1}A_{b1}$
A1			0.030	0.061
A2			0.032	0.065
A3	0.70	0.48–1.00	0.035	0.071
A4			0.038	0.078
A5			0.040	0.082
(b) Higher frequency (HF) group				
Case	f_{p2} (Hz)	$f_{L2} \sim f_{H2}$ (Hz)	A_{b2} (m)	$k_{p2}A_{b2}$
B1			0.030	0.217
B2			0.032	0.231
B3			0.033	0.239
B4	1.34	1.02–1.82	0.035	0.253
B5			0.038	0.268
B6			0.039	0.282
B7			0.040	0.289

experimental process, the data measurement was synchronized with the wavemaker.

B. Experimental parameter

The experiments are composed of two aspects: double-wave-group focusing and its corresponding single-wave-group focusing. In single-wave-group focusing, the assumed focused position and focused time are constant as $x_b = 10$ m and $t_b = 36$ s, respectively. The peak frequency of the lower-frequency (LF) part is fixed as $f_{p1} = 0.70$ Hz and that of the higher-frequency (HF) part is fixed as $f_{p2} = 1.34$ Hz. To facilitate the separation of harmonics in the subsequent analysis, the input spectral bands of these two single wave groups are prescribed not overlapped, one in the range of $[f_{L1}, f_{H1}] = [0.48, 1.00]$ Hz and the other in the range of $[f_{L2}, f_{H2}] = [1.02, 1.82]$ Hz. Different focused amplitudes ranging from 0.03 m to 0.04 m are considered in each

TABLE II. Main parameters of double-wave-group focusing tests. LFF: low-frequency fixed; HFF: high-frequency fixed; and EF: energy fixed.

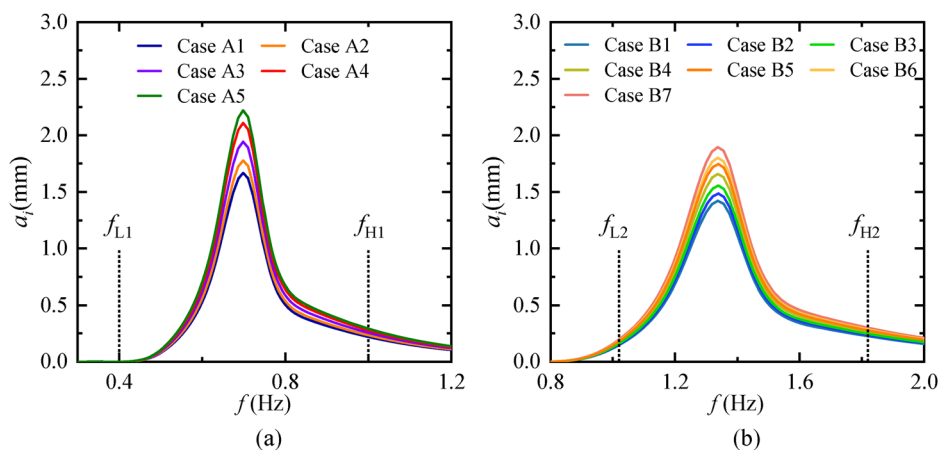
Pattern	Case	A_{b1} (m)	f_{p1} (Hz)	A_{b2} (m)	f_{p2} (Hz)	A_b (m)	A_{b1}^2/A_{b2}^2
LFF	A1B1			0.030		0.060	1.00
	A1B3	0.030	0.70	0.035	1.34	0.065	0.74
	A1B5			0.040		0.070	0.56
HFF	A1B1	0.030		0.030		0.060	1.00
	A3B1	0.035	0.70		1.34	0.065	1.36
	A5B1	0.040				0.070	1.78
EF	A1B6	0.030		0.039		0.069	0.59
	A2B5	0.032		0.037		0.069	0.75
	A3B4	0.035	0.70	0.035	1.34	0.070	1.00
	A4B3	0.038		0.033		0.071	1.33
	A5B2	0.040		0.032		0.072	1.56

group. Detailed parameters are listed in Table I, and the corresponding amplitude spectra are given in Fig. 3.

In double-wave-group focusing, three patterns are covered: low-frequency fixed (LFF), high-frequency fixed (HFF), and energy fixed (EF). Specific combinations and detailed parameters are given in Table II. A_b ($= A_{b1} + A_{b2}$) denotes the estimated focused amplitude of the double-wave-group focusing, i.e., the linear superposition of these two assumed focused amplitudes of the corresponding single-wave-group focusing. Here, A_{b1}^2/A_{b2}^2 is defined to characterize the spectral distribution.

III. GENERATION OF FOCUSED WAVES AND ANALYTICAL METHODOLOGY

Compared with the focused single-wave-group, the spectral bandwidth of fundamental components of the focused double-wave-group is relatively wide, but the evolution of the double-wave-group focusing is different from that of the single-wave-group focusing with a wide spectrum, for much more wave components involved in non-linear focus. In addition to the interaction within a single wave group, there are also interactions between two wave groups, in which energy transfer is significantly complex. How to properly separate these two

**FIG. 3.** Amplitude spectral distribution of single-wave-group focusing tests. (a) Case A and (b) case B.

effects is crucial to accurately understand the mechanism of double-wave-group focusing. The iterative method is preferred over its advantage of correcting the shift of the assumed focused position caused by the nonlinear interactions within the single wave group. In further analysis, the experimental results of two single wave groups (case A5 and case B1) are linearly superposed (named case A5 + case B1) for comparison. Main analytical methodologies such as cross spectrum and wavelet-based bicoherence spectrum used in the following discussion of double-wave-group focusing (case A5B1) and linear superposition (case A5 + case B1) will also be introduced in this section.

A. Harmonic decomposition method

In the physical experiment, the actual focused position always deviates from the prescribed resulting from the nonlinear interactions by wave components within the single wave group. Fitzgerald *et al.*²³ and Buldakov *et al.*²⁹ proposed a methodology consequently and regarded phase correction as the core idea.

According to the wave theory, the free surface elevation up to fourth order can be written as

$$\eta = A\eta_{11} \cos(\theta) + A^2(\eta_{20} + \eta_{22} \cos(2\theta)) + A^3(\eta_{31} \cos(\theta) + \eta_{33} \cos(3\theta)) + A^4(\eta_{40} + \eta_{42} \cos(2\theta) + \eta_{44} \cos(4\theta)) + O(A^5), \quad (1)$$

where A is the wave amplitude. η_{ij} denotes the coefficient of the j times of the i th-order frequency term. Introducing a phase in the form of $\theta + \xi$ and then assigning the value of 0, $\pi/2$, π , and $3\pi/2$ to the phase shift ξ , the expression of η_0 , η_{90} , η_{180} , and η_{270} can be got.³² Based on the intrinsic properties of trigonometric functions, the standard four-phase approach can be decomposed by adding or subtracting from each other.

$$\begin{aligned} S_0 &= \frac{\eta_0 + \eta_{90} + \eta_{180} + \eta_{270}}{4} = A^2\eta_{20} + A^4\eta_{40} + A^4\eta_{44} \cos(4\theta), \\ S_1 &= \frac{\eta_0 + i\eta_{90} - \eta_{180} - i\eta_{270}}{4} = (A\eta_{11} + A^3\eta_{31}) \cos(\theta), \\ S_2 &= \frac{\eta_0 - \eta_{90} + \eta_{180} - \eta_{270}}{4} = (A^2\eta_{22} + A^4\eta_{42}) \cos(2\theta), \\ S_3 &= \frac{\eta_0 - i\eta_{90} - \eta_{180} + i\eta_{270}}{4} = A^3\eta_{33} \cos(3\theta), \end{aligned} \quad (2)$$

where S_0 , S_1 , S_2 , and S_3 denote the nonlinear superharmonics for second (−) and fourth, first (linear), second (+), and third harmonic, respectively. Besides, odd-order harmonics and even-order harmonics can be obtained from $S_1 + S_3$ and $S_0 + S_2$, respectively.

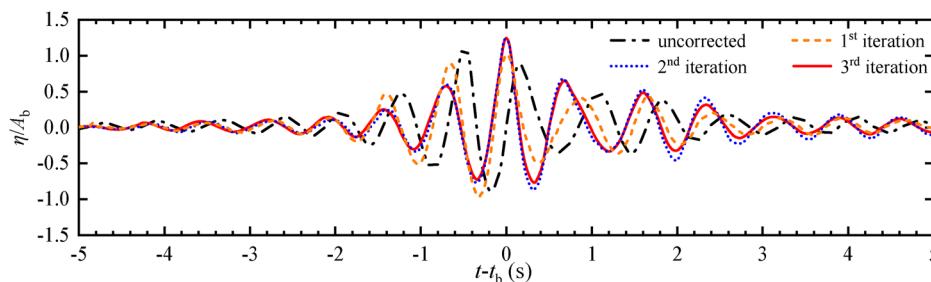


FIG. 4. Comparison of free surface elevation at the assumed focused position before and after correction (case B1: $A_{b2} = 0.030$ m, $f_{p2} = 1.34$ Hz, and $f_{L2} \sim f_{H2} = 1.02 \sim 1.82$ Hz).

B. Iterative method

The measured amplitude a_{out} , achieved by the FFT transform of the linear harmonics S_1 , as well as the target amplitude a_{tgt} is used to calculate the new input amplitude a_{in} , by the same way for the input phases Φ_{in} solution.³³

$$a_{in}^{n+1}(f_i) = a_{in}^n(f_i) a_{tgt}(f_i) / a_{out}^n(f_i), \quad (3)$$

$$\phi_{in}^{n+1}(f_i) = \phi_{in}^n(f_i) + (\phi_{tgt}(f_i) - \phi_{out}^n(f_i)), \quad (4)$$

where the superscript n represents the n th iteration. The procedure is applied iteratively until the linear wave components come into amplitude and phase and the measured linearized spectrum coincides with the target spectrum to the desired accuracy, but the phase is only corrected at the peak frequency. This operation achieves that the actual focused position can be corrected to the prescribed, eliminating the focusing effect caused by the nonlinear interactions within a single wave group, which can be beneficial to the separation of the interactions within and between the wave groups.

In the experiment, the surface elevation information measured at the distance of $x_{amp} = 3.2$ m and $x_b = 10$ m is used for amplitude and phase iteration, respectively. The results of case B1 are taken as an example, shown in Fig. 4. Since phase correction only happens at the peak frequency, it cannot implement that the free surface elevation around the focused time can be coincident in the range of error. Hence, when it comes to this status that the crest reaches the maximum and the adjacent two troughs retain symmetrically, i.e., the free surface elevation after the third iteration shown in Fig. 4 (represented by the solid red line), the correction process is considered to be completed.

For other cases, it needs only a one-time iteration for LF group focusing and a second or third times iteration for HF group focusing to correct the shift of the phase.

C. Cross spectrum

Cross spectrum can quantify the difference in amplitude and phase in the frequency domain based on the free surface elevation time history of case A5B1 and case A5 + case B1, reflecting the correlation information of these two signals. For a stationary random process, the cross-spectral density function $S_{xy}(\omega)$ of the signal $x(t)$ and $y(t)$ is defined as a Fourier transform of the cross correlation function, expressed as

$$S_{xy}(\omega) = C_{xy}(\omega) - iQ_{xy}(\omega), \quad (5)$$

where $C_{xy}(\omega)$ and $Q_{xy}(\omega)$ denote co-spectrum and quadrature spectrum, respectively.

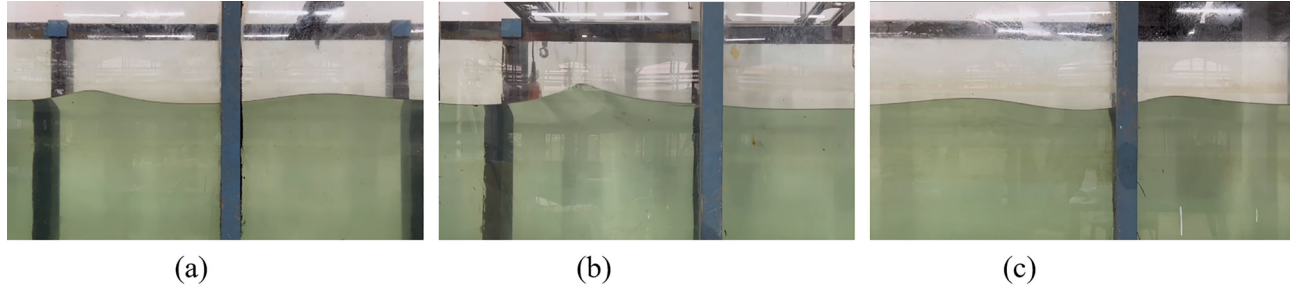


FIG. 5. Experimental photos of the free surface elevation before, at, and behind the focused position. (a) $x = 4.0$, (b) $x = 10.5$, and (c) $x = 15.0$ m.

The difference between the amplitude spectrum and the relative lag of the phase can be reflected by the modulus of cross spectrum $|S_{xy}(\omega)|$ and the phase spectrum $\theta(\omega)$.

$$|S_{xy}(\omega)| = \sqrt{\{C_{xy}(\omega)\}^2 + \{Q_{xy}(\omega)\}^2}, \quad (6)$$

$$\theta(\omega) = \arctan\{Q_{xy}(\omega)/C_{xy}(\omega)\}. \quad (7)$$

D. Wavelet-based bicoherence spectrum

Wavelet-based bicoherence spectrum is an analysis tool to help detect the second-order phase coupling between the frequency components of nonlinear signals, that is, the frequency components that are participated in the bounded nonlinear interactions.

Wavelet-based bicoherence spectrum $b_{Wf}^2(f_1, f_2)$ is defined as³⁴

$$b_{Wf}^2(f_1, f_2) = \frac{B_W^2(f_1, f_2)}{\left[\int_T |WT(f_1, t) WT(f_2, t)|^2 dt \right] \int_T |WT(f_3, t)|^2 dt}, \quad (8)$$

where the subscript W represents the results from the wavelet transform and T represents the duration of the analyzed signal. f_1, f_2 , and f_3 satisfy

$$f_1 + f_2 = f_3. \quad (9)$$

$B_W(f_1, f_2)$ is the second-order wavelet spectrum, given as

$$B_W(f_1, f_2) = \int_T WT(f_1, t) WT(f_2, t) WT^*(f_3, t) dt, \quad (10)$$

in which * represents complex conjugation.

Wavelet-based bicoherence spectrum $b_{Wf}^2(f_1, f_2)$ is valued in the range of 0~1, measuring the proportion of the total energy generated by the secondary phase coupling of f_1 and f_2 in $f_3 = f_1 + f_2$. When $b_{Wf}^2(f_1, f_2) = 1$, it means that the energy in $f_3 = f_1 + f_2$ all comes from the second-order phase coupling of f_1 and f_2 , while $b_{Wf}^2(f_1, f_2) = 0$ means that there is no phase coupling.

IV. COMPARATIVE ANALYSIS OF THE INTERACTIONS INDUCING FOCUSING

Comparative analysis is to be conducted between the information on the double-wave-group focusing at the focused position in the experimental case (case A5B1) and that of the linear superposition (case A5 + case B1) to investigate the nonlinear interactions that lead to focusing.

A. Wave profile

Observed from the photos (Fig. 5) of the free surface elevation before, at, and behind the focused position in the physical experiment of double-wave-group focusing, the focusing process is similar to but not completely to that of single-wave-group focusing. Hereafter, a detailed comparative analysis will be carried out in the time and frequency domain.

Free surface elevation and its corresponding wave spectrum are the direct characteristics. Figure 6 shows the information in the time and frequency domain at the assumed focused position of case A5B1 and case A5 + case B1, along with linear theory for reference.

In Fig. 6(a), the maximum crest of the experimental double-wave-group focusing (case A5B1, represented by the solid red line) is larger than that of linear superposition (case A5 + case B1, represented by dot-dash blue line), followed by the theoretical solution.

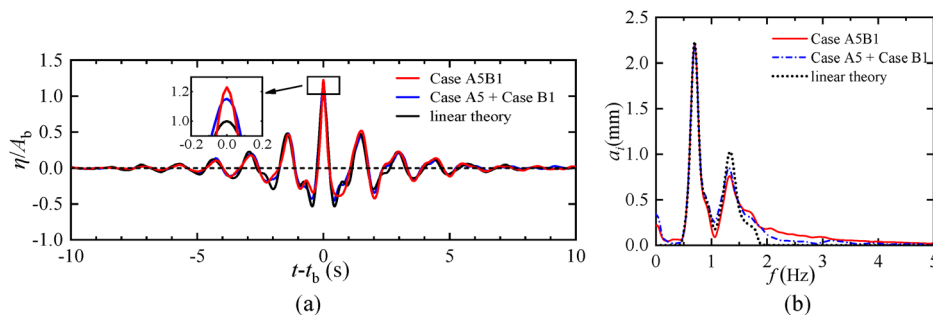


FIG. 6. The comparison of free surface elevations and the corresponding amplitude spectra at the assumed focused position between case A5B1 and case A5 + case B1, along with linear theory for reference. (a) Free surface elevations and (b) amplitude spectra.

Meanwhile, the trough of case A5B1 is the flattest but asymmetrical. This reflects the fact that double-wave-group focusing is not equivalent to the process of linear superposition. Much more wave components must be participated in the nonlinear interaction in experimental double-wave-group focusing, consequently causing frequency components to be focused.

In Fig. 6(b), from the comparison in the frequency domain, fewer distinctive amplitudes are observed in the LF range $[f_{L1}, f_{H1}]$ except for a little in $[f_{p1}, f_{H1}]$, but it is not the same in the GF range $[f_{L2}, f_{H2}]$. The energy transfers from the range of $[f_{L2}, f_{p2}]$ to a higher frequency range, leading to a much wider spectral bandwidth than that of the input spectrum. It is because the steepness of the LF group less than 0.10 is much smaller than that of the GF group. Further, in case A5B1, the energy transfers the most, even spreading up to 4.0 Hz, reflecting that nonlinear interactions occur at the prescribed focused position either in the experimental case or in the linear superposition but are stronger in the former process.

As known, the difference between experimental double-wave-group focusing with linear superposition, as well as linear superposition with linear theory at the focused position, is caused by the interactions between different wave groups (cross-interaction) and interactions within the single wave group (self-interaction), respectively. To describe these differences, cross spectrum is introduced. Figure 7 illustrates the cross spectra of case A5B1 relative to case A5 + case B1 and case A5 + case B1 relative to linear theory, including the amplitude values [Fig. 7(a)] and the phase differences [Fig. 7(b)]. The vertical black dotted lines represent f_{p1} and f_{p2} . The shadow covers the input fundamental frequency range. Considering that the frequency of the linear wave components is within the fundamental frequency range $[f_{L1}, f_{H2}]$, only valid data presented by black scatters in this range are displayed.

In Fig. 7(a), the frequency corresponding to the peak of the HF part shifts downward in the red line, showing a significant phase lag between the experiment case and linear superposition. In Fig. 7(b), in the frequency range $[f_{p1}, f_{H1}]$, there are mainly the phase differences of case A5B1 relative to case A5 + case B1 (represented by red triangles), caused by the interactions between these two wave groups. This can explain why the nonlinear interactions between wave groups dominate the frequency difference in the range $[f_{p1}, f_{H1}]$ shown in Fig. 6(b). In the frequency range $[f_{L2}, f_{H2}]$, both two differences coexist. It reflects

that the frequency difference in Fig. 6(b) was the combined effect of interaction between and within wave groups. While, in the rest frequency range, only phase differences of case A5B1 relative to case A5 + case B1 occur, manifesting that the interactions between wave groups play a leading role in widening the spectral distribution up to 4.0 Hz.

B. Harmonic separation

To further understand the wave components that participated in the focusing process at the focused position, separating the nonlinear superharmonics is quite essential. Figure 8 displays the results of the harmonic separation of double-wave-group focusing, including the experimental result case A5B1 [Fig. 8(a)] and linear superposition case A5 + case B1 [Fig. 8(b)], also with the results of case A5 [Fig. 8(c)] and case B1 [Fig. 8(d)] for reference. The dimensionless surface elevation of the second-order sum and third-order harmonics of case A5B1 is observed to be much larger than that of linear superposition case A5 + case B1.

Figure 9 compares the harmonic components and the corresponding amplitude spectra between case A5B1 and case A5 + case B1. Obtained by the harmonic decomposition method mentioned in Sec. III A, the harmonic components of each order are not completely separated. Here, the focus is on the variation and difference of higher-order frequency multiplication, so the second-order sum [Fig. 9(a)] and third order [Fig. 9(b)] are filtered, while the second-order difference and fourth order [Fig. 9(c)] are not.

In Fig. 9(a), it is quite impressive that the dimensionless maximum crest of the second-order sum at the focused time of case A5B1 is almost as 3.02 times as that of case A5 + case B1, reaching up to the dimensionless value of 0.25, that is, nearly a quarter of the wave crest in linear solution. Note that, due to the limitation of this harmonic separation, a small number of fundamental frequency components cannot be filtered out (f_{p2} is close to $2f_{p1}$) and they are doped in the second-order sum frequency harmonics. This may lead to the dimensionless value being slightly larger than the truth. Meanwhile, concerning the energy in the frequency domain, the results of linear superposition are the sum of interactions within LF and HF groups. Whereas, in the frequency range of $[2f_{p1}, 2f_{p2}]$, the amplitude spectra of case A5B1 are at most one order of magnitude larger than that of case A5 + case B1. This difference comes from the interactions

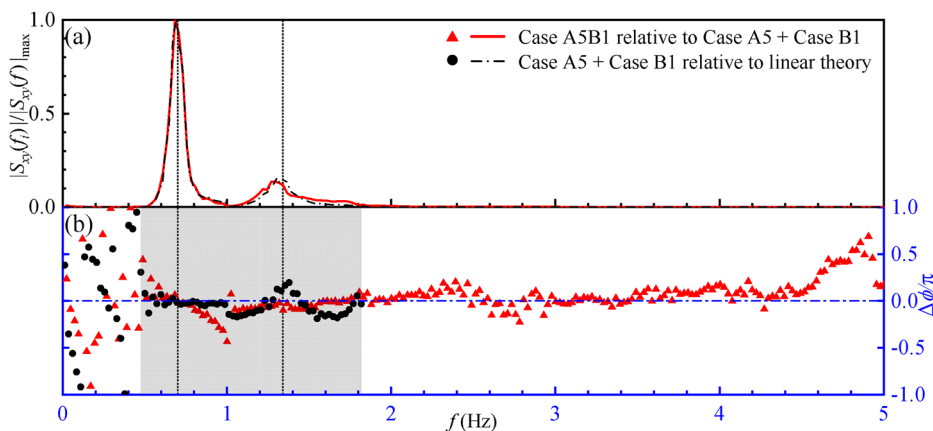


FIG. 7. Cross spectra of case A5B1 relative to case A5 + case B1 and case A5 + case B1 relative to linear theory.

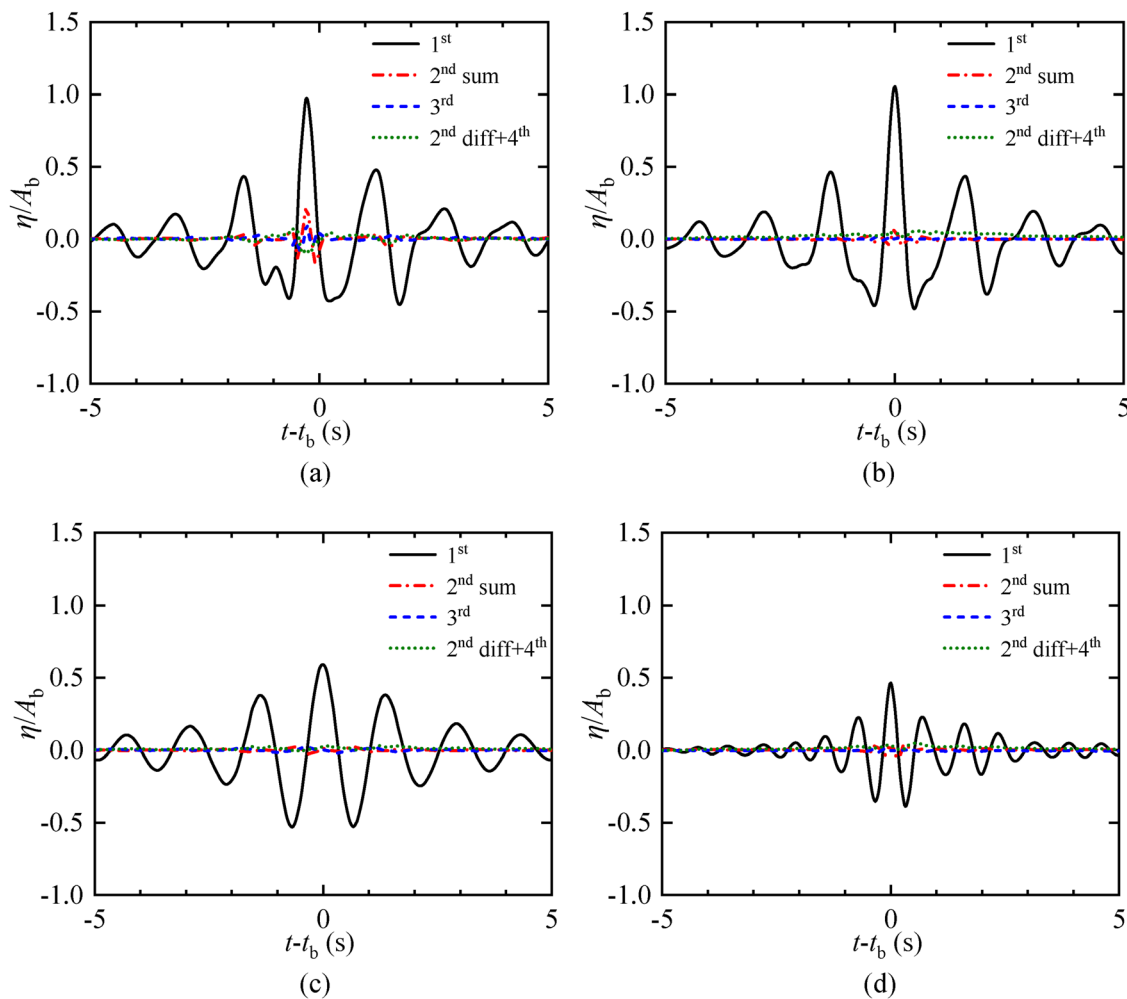


FIG. 8. Harmonic separation of wave-group focusing. (a) case A5B1, (b) case A5 + case B1, (c) case A5, and (d) case B1.

between different wave groups, which is regarded as one of the leading roles in double-wave-group focusing. In Figs. 9(b) and 9(c), for the rest harmonic components, the free surface elevation and the amplitude spectra of case A5B1 are a little larger than those of case A5 + case B1, which plays a relatively minor role in the focusing process.

B. Analysis of the nonlinear interactions coupled

Figure 10 illustrates the wavelet-based bicoherence spectrum of the signals in case A5B1 and case A5 + case B1, a focused single-wave-group (case A5 and case B1) also given for comparison. In the figure, the black lines (and black values) and gray lines represent the peak or multi-peak of the LF group and HF group, respectively. In the experimental double-wave-group focusing [i.e., case A5+B1 in Fig. 10(a)], there is a large area of red in the high-frequency range, indicating that strong interactions happen between the main wave components and the higher-order harmonics, as well as between the higher-order

harmonics and higher-order harmonics. While in the case of the linear superposition [i.e., case A5 + case B1 in Fig. 10(b)], the process is similar to that of the HF group [i.e., case B1 in Fig. 10(d)] focusing, but the frequency band of relatively stronger interaction moves up. There are two relatively stronger interaction bands, [1.4 and 1.6 Hz] and [3.5 and 4.8 Hz], but with a narrower bandwidth. This comparison proves again that double-wave-group focusing is not equivalent to the linear superposition of two single-wave-group focusing, but a more complex physical mechanism undergoing.

To investigate the contribution of harmonics in focused waves, the wavelet-based bicoherence spectrum of each order harmonics is analyzed, as shown in Fig. 11. Since the second difference and fourth-order harmonics are pointed out to play a relatively minor role in the double-wave-group focusing, the corresponding bicoherence spectra are not given. Limited to the harmonic decomposition method, the harmonics are not strictly separated from each other, resulting in high-order sum harmonics mixed with some fundamental components. As shown in the left figures (the results of the experimental

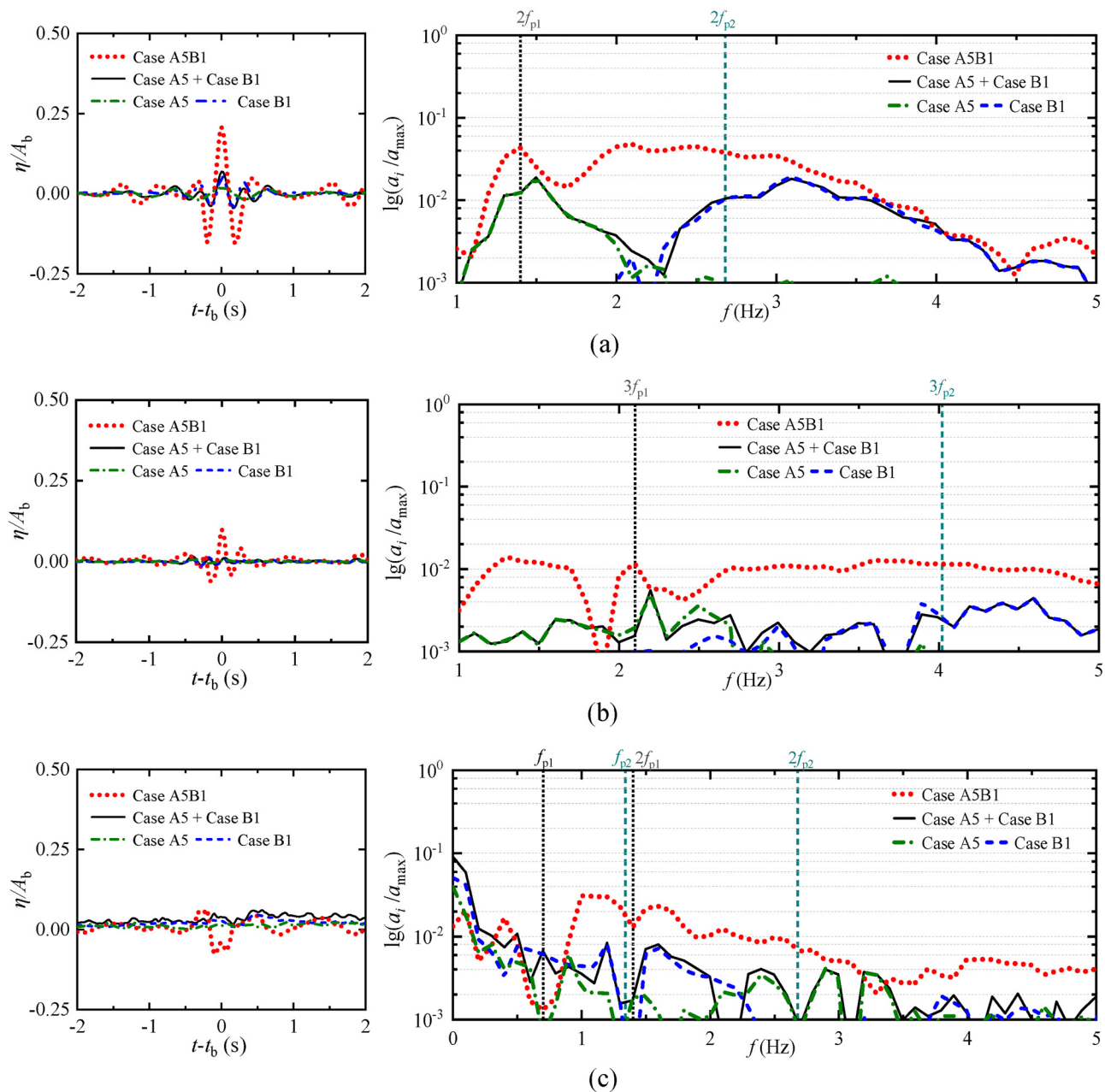


FIG. 9. Comparison of harmonic components and the corresponding amplitude spectra in wave-group focusing. (a) Second-order sum, (b) third order, and (c) second-order difference and fourth order.

case), there is a horizontal interaction band [Fig. 11(b)] caused by the dominant frequency of the LF group and the high-frequency component of the HF group. Here, the interactions between high-order harmonics are the focus of the investigation, so, the horizontal band will not be analyzed in the following study.

From the figure, there is little difference between experimental double-wave-group focusing and linear superposition in the results of linear harmonics [Fig. 11(a)], consistent with the expectations.

Whereas, for the results of the second-order sum [Fig. 11(b)] and third order [Fig. 11(c)], the bicoherence spectrum is quite different, resulting in the different behaviors of the total components. In Fig. 11(b), a strong interaction happens around second-order sum harmonics within the LF group (observed in the right figure), and this interaction extends rightward close to second-order sum harmonics in the LF group with the HF group when it comes to the experimental case. While for the third-order harmonics [Fig. 11(c)], due to the limitation

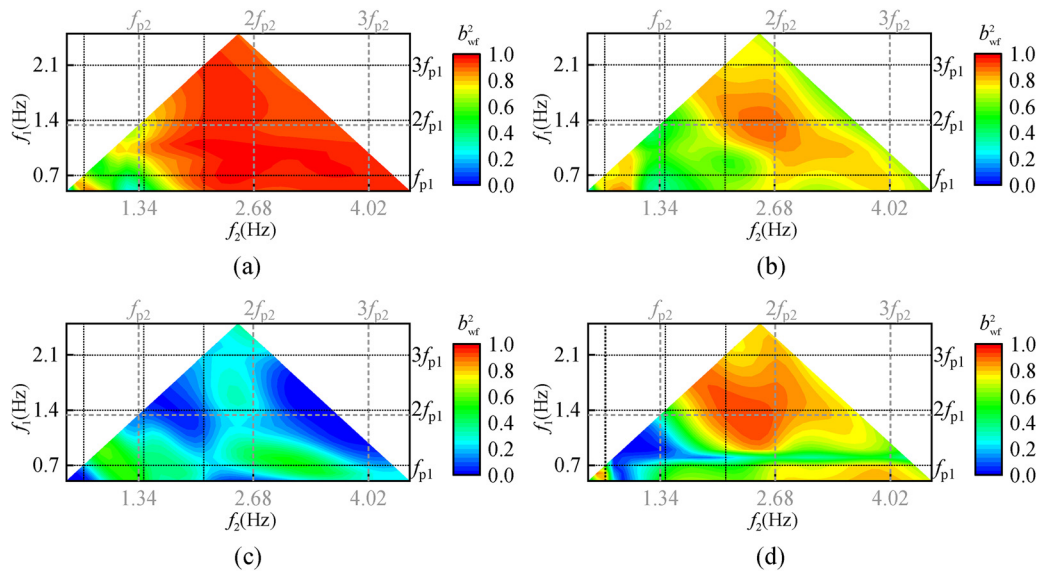


FIG. 10. Wavelet-based bicoherence spectrum of the signals in wave-group focusing. (a) Case A5B1, (b) case A5+caseb1, (c) case A5, and (d) case B1.

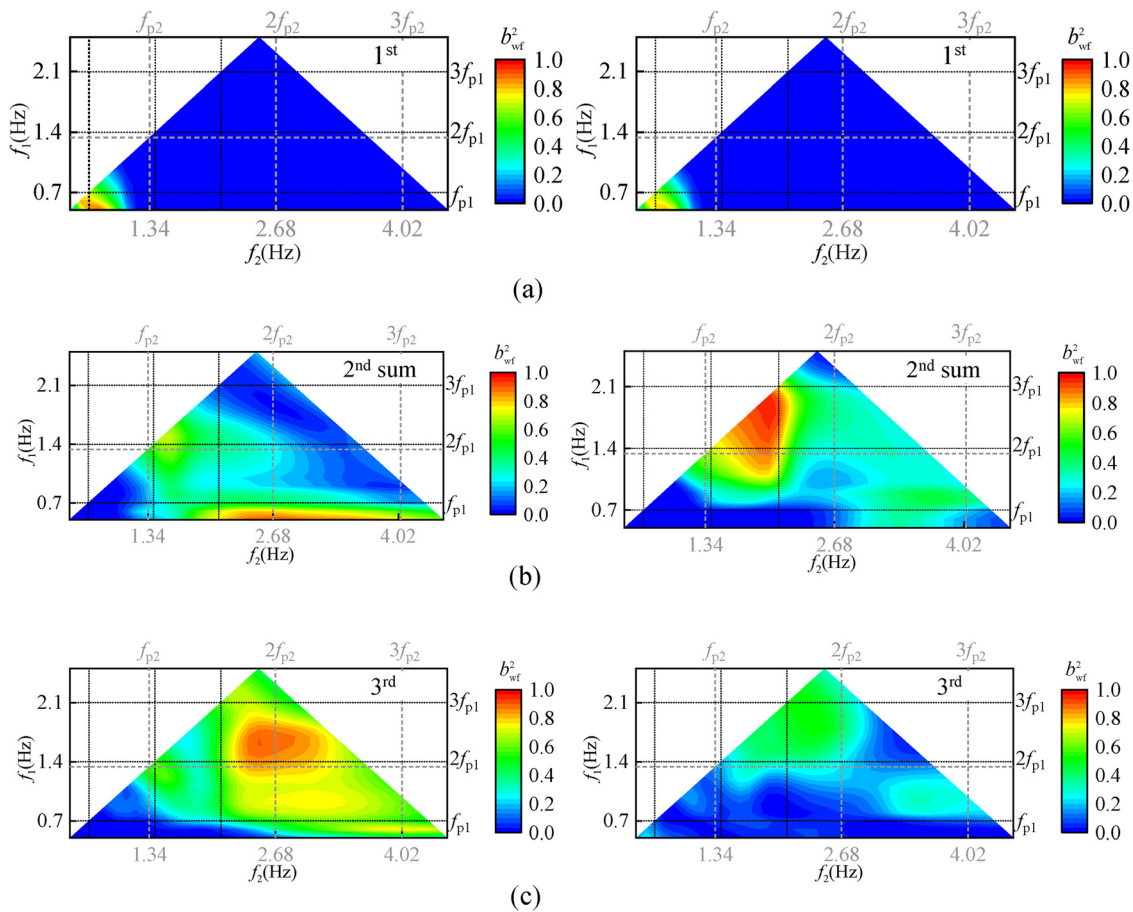


FIG. 11. Wavelet-based bicoherence spectrum of harmonic signals in case A5B1 and case A5 + case B1 (left: case A5B1; right: case A5 + case B1). (a) First order, (b) second-order sum, and (c) third order.

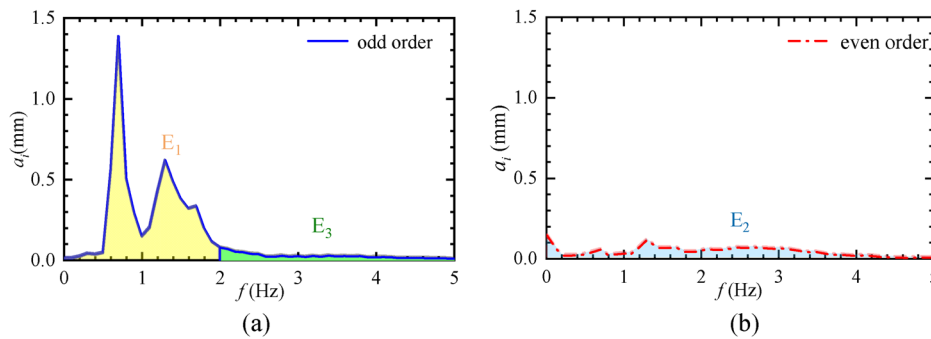


FIG. 12. Schematic diagram of energy division in double-wave-group focusing. (a) Odd-order components and (b) even-order components.

of the truncated frequency range, only a weak interaction band caused by the interactions of third-order harmonics within the LF group can be observed in the right figure, and it moves down with enhancement in the experimental case.

The above findings indicated that the difference in the frequency range [0, 5.0 Hz] between the experimental case and linear superposition is tightly associated with the interactions of second-order sum harmonics involving interactions coming from one wave group or both two wave groups.

V. INFLUENCE OF SPECTRAL DISTRIBUTION ON NONLINEAR INTERACTIONS

Based on the above analysis, the interactions between wave groups cannot be ignored in the double-wave-group focusing. Wave components that participated in the nonlinear interaction are also identified. However, the influences of spectral distribution on the energy transfer and the interactions between wave groups at the focused position are still not clearly understood. Three patterns, such as low-frequency fixed (LFF), high-frequency fixed (HFF), and energy fixed (EF) patterns, are to be investigated in the following study.

A. Energy transfer

Extreme waves are generated at the focused position due to the energy transfer in the process of double-wave-group propagation and evolution. As concluded by Tang *et al.*,³⁵ the rogue wave density is closely related to the high-frequency tails, showing that the high-frequency tails are quite essential to extreme events. To study the energy transfer in cases with different spectral distributions, the total energy $E_0 (= E_1 + E_2 + E_3)$ is divided into three parts: one in the linear frequency band E_1 , another in even-order frequency band E_2 , and the last in high-frequency tail E_3 , illustrated in Fig. 12.

The energy ratio in each frequency band at the focused position considering different patterns is displayed in Fig. 13. Solid scatters denote the results of experimental cases, and hollow scatters denote the results of linear superposition.

In Fig. 13(a), the case is categorized as the LFF pattern, in which A_{b1} is fixed but A_{b2} variable. In experimental cases, with the increase in A_{b1}^2/A_{b2}^2 (the decrease in A_{b2}), the value of E_1/E_0 gradually increases from 0.65 to 0.71, and the value of E_2/E_0 and E_3/E_0 decreases from 0.24 to 0.21 and from 0.11 to 0.08, respectively. The trend of linear superposition is quite similar. Yet/However, the value of E_2/E_0 and E_3/E_0 decreases from 0.14 to 0.13 and from 0.06 to 0.05, respectively.

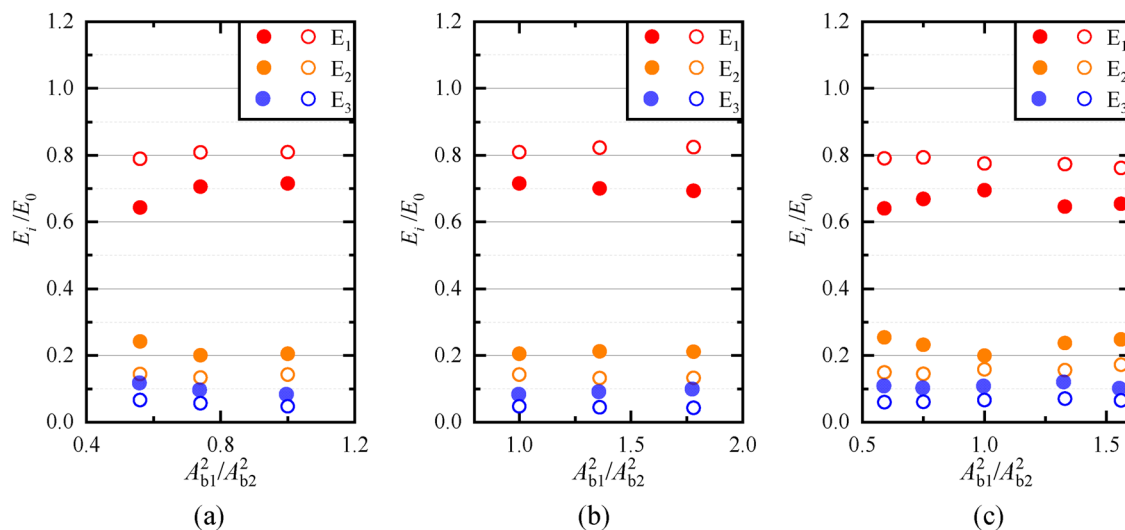


FIG. 13. Comparison of the energy ratio in each frequency band at the focused position in double-wave-group focusing tests with three different patterns (solid scatters: experimental case; hollow scatters: linear superposition). (a) LFF, (b) HFF, and (c) EF.

This makes perfect sense. The larger the value of A_{b2} (the smaller value of A_{b1}^2/A_{b2}^2), the larger the energy of the HF group, and the more nonlinearity and the stronger interaction the mixed system possess.

In Fig. 13(b), the value of A_{b2} is fixed, but the value of A_{b1} is changeable, named HFF pattern. In both two cases, the energy ratio in each frequency band hardly changes as the value of A_{b1}^2/A_{b2}^2 increases (the value of A_{b1} increases). It is because the LF group has weak nonlinearity, with steepness valued less than 0.10. This reflects that the nonlinear impact depends more on the HF components, which is sort of coincident with what was found on the impact of HF tails by Tang *et al.*³⁵

In Fig. 13(c), in the EF pattern, something different happens. As the value of A_{b1}^2/A_{b2}^2 increases, the energy ratio of each order harmonics shows a nonmonotonic variation. When the value of A_{b1}^2/A_{b2}^2 is smaller than 1.0, the larger the value of A_{b1}^2/A_{b2}^2 , the more the linear superposition and the less the nonlinear interaction. It is similar to the results of the LFF pattern with A_{b1}^2/A_{b2}^2 less than 1.0. When the value of A_{b1}^2/A_{b2}^2 is larger than 1.0, the value of E_2/E_0 increases as the value of A_{b1}^2/A_{b2}^2 increases. Different from the HFF pattern, under the assumption of equivalent energy, the nonlinearity of the long-wavelength wave components (i.e., components in the LF group)

is enhanced and the long-wavelength wave components contribute to nonlinear interaction more. It means that in the EF pattern, the more asymmetrical the spectral distribution, the less nonlinear superposition, and the more nonlinear interaction.

B. Participation in nonlinear interactions

To explore the impact of asymmetry of spectral distribution on the evolution of double-wave-group focusing and well understand the components involved in nonlinear interactions, the wavelet-based bicoherence spectra of the total wave components and the high-order harmonics of the experimental case and linear superposition in EF pattern are analyzed in Figs. 14 and 15, including wind-sea dominated, sea-swell energy equivalent, and swell-dominated typical wave configurations.

In Fig. 14, the difference between the results of the experimental case and the linear superposition is outstanding. There are still much more interactions and stronger nonlinearity in the former process. While for the results of linear superposition, in wind-sea-dominated [Fig. 14(a)] and swell-dominated [Fig. 14(c)] states, the stronger interaction coupled presents as an inclined ribbon distributed above 4 Hz.

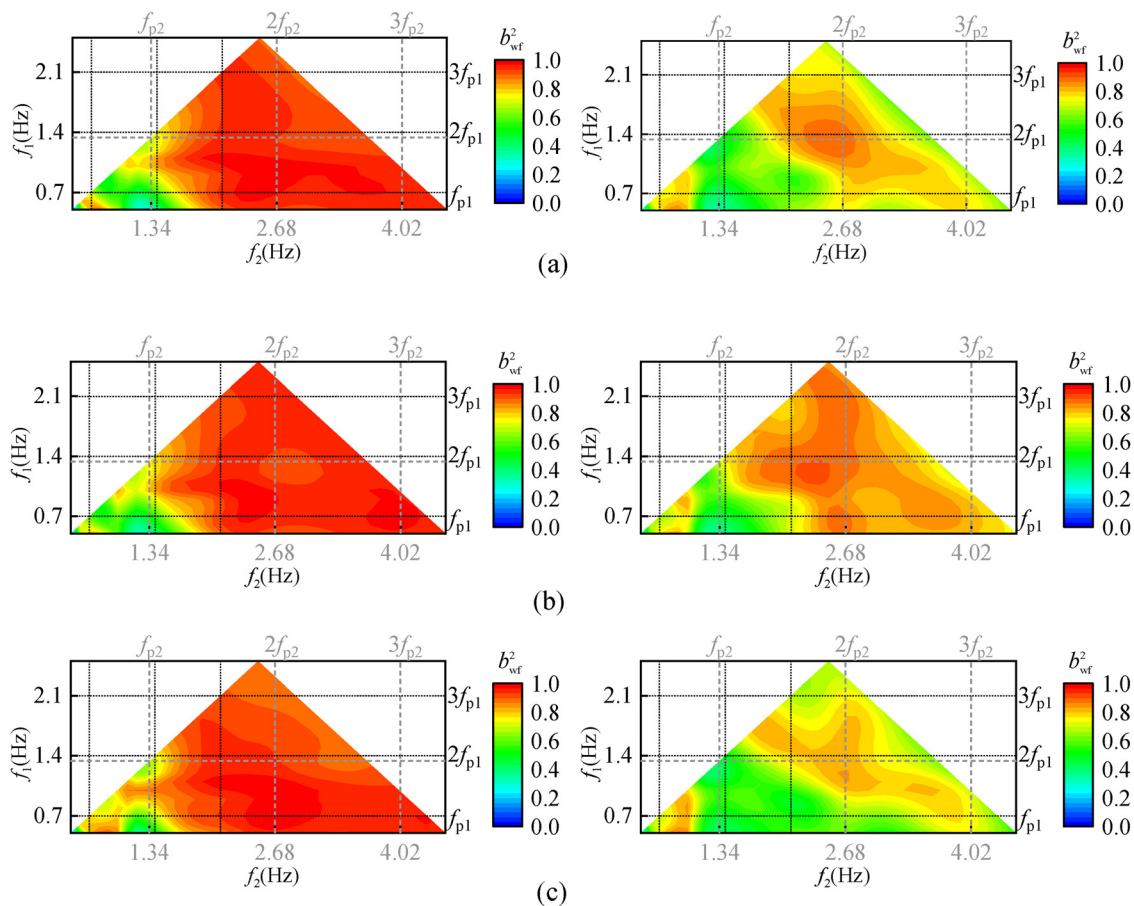


FIG. 14. The variation of wavelet-based bicoherence spectra of total wave components of the experimental case and linear superposition (left: experimental case; right: linear superposition). (a) $A_{b1}^2/A_{b2}^2 = 0.59$ (wind-sea-dominated), (b) $A_{b1}^2/A_{b2}^2 = 1.00$ (sea-swell energy equivalent), and (c) $A_{b1}^2/A_{b2}^2 = 1.56$ (swell-dominated).

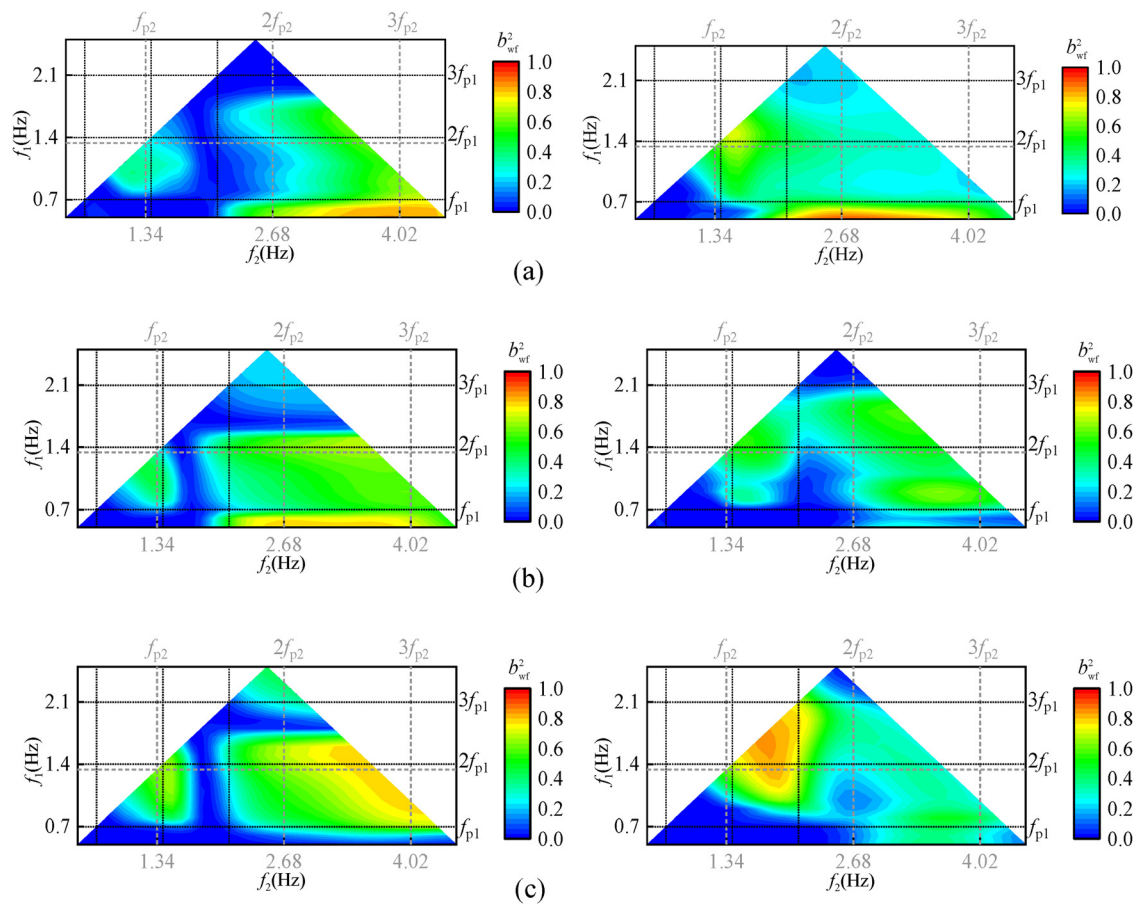


FIG. 15. The variation of wavelet-based bicoherence spectra of second sum frequency components of the experimental case and linear superposition (left: experimental case; right: linear superposition). (a) $A_{b1}^2/A_{b2}^2 = 0.59$ (wind-sea-dominated), (b) $A_{b1}^2/A_{b2}^2 = 1.00$ (sea-swell energy equivalent), and (c) $A_{b1}^2/A_{b2}^2 = 1.56$ (swell-dominated).

This can be explained by the asymmetric spectral distribution, which leads to the strength of the interaction being determined by the dominant system. While in the sea-swell energy equivalent state [Fig. 14(b)], the spectral band moves downward, indicating that the interaction within the two wave groups may be superimposed.

Compared the results of the experimental case with that of linear superposition, it can be observed that in the sea-swell energy equivalent state, the interactions within wave groups are the strongest and the interactions between wave groups are the weakest, which is also consistent with the above conclusions in Sec. V A. That is, for the sea stats with asymmetrical spectral distribution, there seems to be more interaction and stronger nonlinearity between wave groups.

In Secs. IV B and IV C, it reveals that the second-order sum harmonics are of vital importance in double-wave-group focusing. Here, for further information on the influence of spectral distribution on nonlinear interaction that induces focusing, the wavelet-based bicoherence spectra of second-order sum harmonics of the experimental case are compared with that of linear superposition, given in Fig. 15.

In detail, in the wind-sea-dominated state [Fig. 15(a)], there are quite weak interactions between two wave groups (i.e., the interactions around between the second-order sum of the LF group and the second-order sum of the HF group) and weak interaction of the

second-order sum within the LF group. This reflects that when the long waves (corresponding to the waves in the LF group) with relatively less energy are coherent with the short waves (corresponding to the waves in the HF group) with relatively more energy, the interaction of second-order sum harmonics in the mixed system mainly comes from those within the HF groups.

In the sea-swell energy equivalent state [Fig. 15(b)], the interactions between two wave groups become strong, and the strength of the coupled interaction is relatively uniform, with no obvious dominance. It means that when the long waves are coherent with the short waves with the equivalent energy, the interactions of second-order sum harmonics come from both within and between the HF group and the LF group.

In the swell-dominated state [Fig. 15(c)], a strong interaction band emerged by the interactions of second-order sum harmonics between the LF group and HF group in the experimental case, and another is caused by the interactions of second-order sum harmonics within the LF group in the right figure. It shows that when the long waves with relatively more energy are coherent with the short waves with relatively less energy, the interaction of second-order sum harmonics between wave groups is strong, and the nonlinearity of the mixed system mainly comes from the interactions within the LF groups and the interactions between LF group and HF group.

Based on the above analysis, it can be summarized that when the long waves are coherent with the short waves, the spectral distribution (energy distribution) has a great impact on the interaction in double-wave-group focusing. When the energy of the LF group is more than that of the HF group (i.e., the swell-dominated state), the interactions of second-order sum harmonics between the LF group and HF group cannot be ignored in studying double-wave-group focusing.

VI. CONCLUSIONS

In this paper, experiments of double-wave-group focusing and their corresponding single-wave-group focusing are conducted. The linear superposition of the wavemaker signals of the corresponding single-wave-group focusing obtained by the iterative method is beneficial for the decomposition of the interaction between two focused wave groups and within a single wave group. The difference between these two interactions as well as the participation of the nonlinear effect is analyzed. The influences of the spectral distribution on energy transfer and nonlinear interactions are also compared. The main conclusions are as follows:

- (1) The physical process of double-wave-group focusing is not simply equivalent to a linear superposition of the corresponding single-wave-group focusing. The former manifests a much sharper crest and more asymmetrical trough in the time domain, and a much wider spectral bandwidth in the frequency domain.
- (2) Second-order sum harmonics is the dominant difference between experimental case and linear superposition. Based on the harmonic decomposition method, linear, second-order sum, third order, and second-order difference and fourth-order components are separated. The dimensionless maximum crest of the second-order sum in case A5B1 is nearly 3.02 times that in case A5 + case B1. And in the frequency range of $[2f_{p1}, 2f_{p2}]$, the amplitude spectra of case A5B1 are at most one order of magnitude larger than that of case A5 + case B1.
- (3) In the low-frequency fixed (LFF) pattern, the larger the energy of the higher-frequency group, the more nonlinearity and the stronger interaction the mixed system possess. While in the high-frequency fixed (HFF) pattern, the energy ratio in each frequency band hardly changes with the variation of the energy of the lower-frequency group, reflecting that the nonlinear impact depends on the higher-frequency tails.
- (4) Under the assumption of equivalent energy, the more asymmetrical the spectral distribution, the less linear superposition, and the more nonlinear interaction. That is, in the sea-swell energy equivalent state, the strength of interactions between wave groups is the weakest.
- (5) When the long-wavelength waves are coherent with the short-wavelength waves, the spectral distribution has a great impact on the interaction in double-wave-group focusing. The interactions of second-order sum harmonics between the lower-frequency group and higher-frequency group cannot be ignored in the swell-dominated state.

The above findings show that the previous explanations of the narrower bandwidth configuration are not available for a bimodal sea state. The interactions between wave groups are not exactly the same as the interactions within a single wave group, promoting the understanding of the generation mechanism of extreme waves.

However, to fully understand the nonlinear interaction between wave groups, it is necessary to analyze the physics in sea states with various wave configurations. Limited by the experimental conditions in this paper, only the mechanism under fixed spectral peak frequency is studied, and no other groups of experiments and analyses were carried out. This causes the above conclusion drawn available under certain conditions. In addition, the analysis was only conducted at the prescribed focused position, with no analysis of wave propagation and evolution, which is also a more noteworthy topic on extreme waves. In the following work, further studies will be improved by numerical simulation based on a fully nonlinear method.

ACKNOWLEDGMENTS

This work is supported by the National Natural Science Foundation of China (Nos. 52071096 and 52201322), the National Natural Science Foundation of China National Outstanding Youth Science Fund Project (No. 52222109), Guangdong Basic and Applied Basic Research Foundation (No. 2022B1515020036), the Fundamental Research Funds for the Central Universities (No. 2022ZYGXZR014), and EPSRC (No. EP/V050079/1).

AUTHOR DECLARATIONS

Conflict of Interest

The authors have no conflicts to disclose.

Author Contributions

Binzhen Zhou: Conceptualization (lead); Funding acquisition (lead); Project administration (lead); Supervision (lead); Writing – review & editing (equal). **Kanglixi Ding:** Conceptualization (equal); Data curation (lead); Investigation (lead); Methodology (equal); Visualization (equal); Writing – original draft (lead). **Jiahao Wang:** Formal analysis (equal); Investigation (equal); Visualization (equal). **Lei Wang:** Conceptualization (equal); Formal analysis (equal); Methodology (lead); Writing – review & editing (equal). **Peng Jin:** Formal analysis (equal); Writing – review & editing (equal). **Tianning Tang:** Methodology (equal); Writing – review & editing (equal).

DATA AVAILABILITY

The data that support the findings of this study are available from the corresponding author upon reasonable request.

APPENDIX: WAVEMAKER CONDITIONS

For double-wave-group focusing tests, the wavemaker signals were achieved by the linear superposition of their corresponding single-wave-group focusing cases. About linear wave-maker theory, the wavemaker's motion of single-wave-group focusing $X(t)$ can be determined by the target free surface elevation η at $x=0$ and the linear transfer function $T_r(f_i)$

$$X(t) = \int \frac{\omega}{T_r(f_i)} \eta(x=0, t), \quad (\text{A1})$$

in which free surface elevation $\eta(x, t)$ can be expressed as Rapp and Melville:³⁶

$$\eta(x, t) = \sum_{i=1}^N a_i \cos(k_i(x - x_b) - 2\pi f_i(t - t_b)), \quad (\text{A2})$$

where the subscript i represents the i th wave component and N denotes the total wave number. x_b and t_b are the assumed focused position and focused time, respectively. The wave frequency f_i is uniformly distributed in the frequency range of $[f_L, f_H]$ (f_L represents the upper and f_H represents the lower). The wave number k_i can be obtained through the dispersion equation,

$$(2\pi f_i)^2 = gk_i \tanh k_i d. \quad (\text{A3})$$

The wave amplitude a_i depends on the wave spectrum $S(f_i)$,

$$a_i = \frac{S(f_i)}{\sum_{i=1}^N S(f_i)} A_b, \quad (\text{A4})$$

in which A_b is the assumed focused amplitude. The JONSWAP spectrum $S(f)$ is defined by the Joint North Sea Wave Project wave spectrum (NJS),³⁷ expressed as

$$S(f) = \beta_1 H_{1/3}^2 T_p^{-4} f^{-5} \exp \left[-\frac{5}{4} (T_p f)^{-4} \right] \gamma^{\exp \left[(f/f_p - 1)^2 / 2\sigma^2 \right]}, \quad (\text{A5})$$

where $\beta_1 = 0.06238 / [0.230 + 0.0336\gamma - 0.185(1.9 + \gamma)] (1.094 - 0.01915 \ln \gamma)$. $\sigma = 0.07$ ($f < f_p$) and $\sigma = 0.09$ ($f \geq f_p$). $H_{1/3}$ is the significant wave height. T_p is the peak period corresponding to the peak frequency f_p . The shape parameter $\gamma = 3.3$ is used in this study.

The linear transfer function of the plate-type wave maker is given as follows:

$$T_r(f_i) = \frac{4 \sinh^2(k_i d)}{2k_i d + \sinh(2k_i d)}. \quad (\text{A6})$$

REFERENCES

- ¹K. B. Dysthe, "Note on a modification to the nonlinear Schrödinger equation for application to deep water waves," *Proc. R. Soc. A* **369**(1736), 105–114 (1979).
- ²I. Nikolkina and I. Didenkulova, "Rogue waves in 2006–2010," *Nat. Hazards Earth Syst. Sci.* **11**(11), 2913–2924 (2011).
- ³A. Toffoli, J. M. Lefèvre, E. Bitner-Gregersen *et al.*, "Towards the identification of warning criteria: Analysis of a ship accident database," *Appl. Ocean Res.* **27**(6), 281–291 (2005).
- ⁴M. Onorato, S. Residori, U. Bortolozzo *et al.*, "Rogue waves and their generating mechanisms in different physical contexts," *Phys. Rep.* **528**(2), 47–89 (2013).
- ⁵L. Wang, B. Zhou, P. Jin, J. Li, S. Liu, and G. Ducroz, "Relation between occurrence probability of freak waves and kurtosis/skewness in unidirectional wave trains under single-peak spectra," *Ocean Eng.* **248**, 110813 (2022).
- ⁶L. Wang, K. Ding, B. Zhou, J. Li, S. Liu, and T. Tang, "Quantitative prediction of the freak wave occurrence probability in co-propagating mixed waves," *Ocean Eng.* **271**, 113810 (2023).
- ⁷L. Wang, J. Li, S. Liu, and G. Ducroz, "Statistics of long-crested extreme waves in single and mixed sea states," *Ocean Dyn.* **71**, 21–42 (2021).
- ⁸C. Kharif, E. Pelinovsky, and A. Slunyaev, *Rogue Waves in the Ocean* (Springer, Berlin, Heidelberg, 2009).
- ⁹C. Kharif and E. Pelinovsky, "Physical mechanisms of the rogue wave phenomenon," *Eur. J. Mech., B* **22**(6), 603–634 (2003).
- ¹⁰K. Dysthe, H. E. Krogstad, and P. Müller, "Oceanic rogue waves," *Annu. Rev. Fluid Mech.* **40**, 287–310 (2008).
- ¹¹T. A. A. Adcock and P. H. Taylor, "The physics of anomalous ('rogue') ocean waves," *Rep. Prog. Phys.* **77**(10), 105901 (2014).
- ¹²T. B. Benjamin and J. E. Feir, "The disintegration of wave trains on deep water. Part 1: Theory," *J. Fluid Mech.* **27**(3), 417–430 (1967).
- ¹³P. A. E. M. Janssen, "Nonlinear four-wave interactions and freak waves," *J. Phys. Oceanogr.* **33**(4), 863–884 (2003).
- ¹⁴M. Onorato, A. R. Osborne, M. Serio *et al.*, "Observation of strongly non-Gaussian statistics for random sea surface gravity waves in wave flume experiments," *Phys. Rev. E* **70**(6), 67302 (2004).
- ¹⁵N. Mori and P. A. E. M. Janssen, "On kurtosis and occurrence probability of freak waves," *J. Phys. Oceanogr.* **36**(7), 1471–1483 (2006).
- ¹⁶R. S. Gibson and C. Swan, "The evolution of large ocean waves: The role of local and rapid spectral changes," *Proc. R. Soc. A* **463**(2077), 21–48 (2007).
- ¹⁷G. Dong, Y. Ma, M. Perlin, X. Ma, Y. Bo, and J. Xu, "Experimental study of wave-wave nonlinear interactions using the wavelet-based bicoherence," *Coastal Eng.* **55**(9), 741–752 (2008).
- ¹⁸A. Tao, J. Zheng, B. Chen, H. Li, and J. Peng, "Properties of freak waves induced by two kinds of nonlinear mechanisms," *Coastal Eng. Proc.* **1**(33), 73 (2012).
- ¹⁹Y. Li, Y. Zheng, Z. Lin, T. A. A. Adcock, and T. S. Van den Bremer, "Surface wavepackets subject to an abrupt depth change. Part 1. Second-order theory," *J. Fluid Mech.* **915**, A71 (2021).
- ²⁰T. Tang, P. S. Tromans, and T. Adcock, "Field measurement of nonlinear changes to large gravity wave groups," *J. Fluid Mech.* **873**, 1158–1178 (2019).
- ²¹J. Xie, Y. Ma, G. Dong, and M. Perlin, "Numerical investigation of third-order resonant interactions between two gravity wave trains in deep water," *Phys. Rev. Fluids* **6**, 014801 (2021).
- ²²J. R. Chaplin, "On frequency-focusing unidirectional waves," *Int. J. Offshore Polar Eng.* **6**(2), 131–137 (1996).
- ²³C. J. Fitzgerald, P. H. Taylor, R. E. Taylor *et al.*, "Phase manipulation and the harmonic components of ringing forces on a surface-piercing column," *Proc. R. Soc. A* **470**(2168), 20130847 (2014).
- ²⁴T. E. Baldock and C. Swan, "Extreme waves in shallow and intermediate water depths," *Coastal Eng.* **27**(1–2), 21–46 (1996).
- ²⁵T. B. Johannessen and C. Swan, "A laboratory study of the focusing of transient and directionally spread surface water waves," *Proc. R. Soc. A* **457**(2008), 971–1006 (2001).
- ²⁶A. Yao and C. H. Wu, "Incipient breaking of unsteady waves on sheared currents," *Phys. Fluids* **17**, 082104 (2005).
- ²⁷C. Schmittner, S. Kosleck, and J. Hennig, "A phase-amplitude iteration scheme for the optimization of deterministic wave sequences," *Int. Conf. Offshore Mech. Arctic Eng.* **6**, 653–660 (2009).
- ²⁸H. Fernandez, V. Sriram, S. Schimmels, and H. Oumeraci, "Extreme wave generation using self-correcting method-revisited," *Coastal Eng.* **93**, 15–31 (2014).
- ²⁹E. Buldakov, D. Stagonas, and R. Simons, "Extreme wave groups in a wave flume: Controlled generation and breaking onset," *Coastal Eng.* **128**, 75–83 (2017).
- ³⁰C. G. Soares, "Representation of double-peaked sea wave spectra," *Ocean Eng.* **11**(2), 185–207 (1984).
- ³¹C. G. Soares, "On the occurrence of double peaked wave spectra," *Ocean Eng.* **18**(1–2), 167–171 (1991).
- ³²L. F. Chen, D. Stagonas, H. Santo *et al.*, "Numerical modelling of interactions of waves and sheared currents with a surface piercing vertical cylinder," *Coastal Eng.* **145**, 65–83 (2019).
- ³³D. Stagonas, P. Higuera, and E. Buldakov, "Simulating breaking focused waves in CFD: Methodology for controlled generation of first and second order," *J. Waterw., Port, Coastal, Ocean Eng.* **144**(2), 06017005 (2018).
- ³⁴J. Chung and E. J. Powers, "The statistics of wavelet-based bicoherence," in *Proceedings of the IEEE-SP International Symposium on Time-Frequency and Time-Scale Analysis* (IEEE, 1998), pp. 141–144.
- ³⁵T. Tang, D. Barratt, H. Bingham, T. S. Van den Bremer, and T. A. A. Adcock, "The impact of removing the high-frequency spectral tail on rogue wave statistics," *J. Fluid Mech.* **953**, A9 (2022).
- ³⁶R. J. Rapp and W. K. Melville, "Laboratory measurements of deep-water breaking waves," *Philos. Trans. R. Soc., A* **331**(1622), 735–800 (1990).
- ³⁷Y. Goda, "A comparative review on the functional forms of directional wave spectrum," *Coastal Eng. J.* **41**(1), 1–20 (1999).